Fizika Nizkikh Temperatur, 2008, v. 34, No. 11, p. 1167–1176

Electronic structure and bulk properties of MB_6 and MB_{12} borides

G.E. Grechnev, A.E. Baranovskiy, V.D. Fil, T.V. Ignatova, I.G. Kolobov, and A.V. Logosha

B. Verkin Institute for Low Temperature Physics and Engineering of the National Academy of Sciences of Ukraine
47 Lenin Ave., Kharkov 61103, Ukraine
E-mail: grechnev@ilt.kharkov.ua

N.Yu. Shitsevalova and V.B. Filippov

Institute for Problems of Materials Science of the National Academy of Sciences of Ukraine
3 Krzhyzhanovsky Str., Kiev 03680, Ukraine

Olle Eriksson

Department of Physics, University of Uppsala, Box 530, SE-751 21 Uppsala, Sweden

Received May 21, 2008

Ab initio band structure calculations have been carried out for higher borides MB_6 and MB_{12}. High precision measurements of the elastic constants were performed for ZrB_{12}, HoB_{12}, ErB_{12}, TmB_{12}, LuB_{12}, YB_6 and LaB_6 compounds at low temperatures. The bulk properties of the borides have been analyzed on the basis of the calculated equations of states and balanced crystal orbital overlap populations. Our calculations indicate that hexaborides with divalent metals, CaB_6, SrB_6, BaB_6, and YbB_6, are semiconductors with small energy gaps. The metallic MB_6 hexaborides with trivalent M atoms are found to possess larger bulk moduli values. For dodecaborides bulk moduli are found to be higher for MB_{12} with increased filling of the conduction band (ZrB_{12}, HfB_{12}, UB_{12}), comparatively to $M^{3+}B_{12}$ compounds. The total energy calculations for different magnetic configurations in YbB_{12} point to a possibility of antiferromagnetic coupling between Yb^{3+} ions.

PACS: 62.20.D– Elasticity;
71.15.Nc Total energy and cohesive energy calculations;
71.20.Lp Intermetallic compounds.

Keywords: rare-earth compounds, borides, bulk properties, electronic structure.

Introduction

The discovery of superconductivity (SC) in MgB_2 at $T_{SC} \simeq 40$ K has stimulated intensive investigations of boron-rich compounds. Among them, the MB_6 hexaborides and MB_{12} dodecaborides (M is alkaline-earth, rare-earth, early transition, or actinide metal) exhibit a wide range of peculiar physical properties [1–3], such as SC (YB_6 and ZrB_{12}, Refs. 1, 4–8), Kondo and valence fluctuation effects (CeB_6, SmB_6, and YbB_{12}, Refs. 9–11), colossal magnetoresistance (EuB_6 [12–14]), and narrow gap semiconducting behavior (YbB_6 [15,16]). Some hexaborides are expected to be candidates for thermoelectric conversion materials with very promising applications [17]. At the same time, there are scarce and conflicting published data on the elastic properties of hexaborides.

Also, ferromagnetism (FM) was recently reported at high temperatures in La doped alkaline-earth hexaboride compounds [18] (and later in CaB_2C_2 [19]), and the origin of this effect is still under discussion. The recent experimental and theoretical results related to anomalous FM of these borides and their electronic spectra are given in Refs. 20–25 and in the references therein. In addition, the trivalency of some fraction of Yb atoms and a related possibility of FM state in YbB_6 have been reported [16]. Obviously, the magnetic semiconducting borides attract a

considerable attention in the novel field of spintronics [20].

With the exception of YbB_{12}, information on physical properties of the dodecaborides is still scarce. It was recently found, that heavy rare-earth (RE) dodecaborides demonstrate anomalous magnetic [26] and thermal [27,28] properties. The dodecaborides are considered as hard and refractory materials, and these properties are related to peculiar chemical bonding in such compounds. However, little is known about elastic properties of MB_{12}. In general, the MB_6 and MB_{12} borides are of great scientific interest and technological importance due to their extraordinary electronic, magnetic, and structural properties. Remarkably, that compounds with comparatively simple cubic crystal structures possess such variety of physical properties.

In the present work we are focused on theoretical and experimental studies of electronic structure and bulk properties of two series of borides, MB_6 (M = Y, Ca, Sr, Ba, La, Eu, Gd, Yb) and MB_{12} (M = Y, Zr, Ho, Er, Tm, Yb, Lu, Hf, Th, U). In order to shed light on the origin of the intriguing properties of these borides, the corresponding *ab initio* calculations of electronic structures are carried out within consistent and reliable computational techniques. In the experimental part, the high-precision measurements of the lattice parameters and elastic constants have been performed for ZrB_{12}, HoB_{12}, ErB_{12}, TmB_{12}, LuB_{12}, YB_6 and LaB_6 borides. The main objective of these studies was to determine the principal electronic states and interactions responsible for the bulk properties of the representative compounds of MB_6 and MB_{12} series. The effects of magnetic interactions, magnetic ordering, and superconductivity have been also addressed, when it was pertinent. Also, a comparison of the experimental data and the calculated volume dependent band structures is expected to be very useful for development of advanced theoretical models for electronic structure of rare-earth compounds.

Experimental details

The process of sample preparation consists of the synthesis of dodecaborides by a borothermal reduction of the metal oxides in vacuum at 1900 K, the compacting of these powders into rods and their subsequent sintering, and of inductive zone melting. The purity of the initial oxides M_2O_3 was 4N. The content of the main substance in the initial amorphous boron was no less than 99.5%. Highly volatile impurities in boron were deleted partially during the synthesis procedure and partially during zone melting. The total content of impurities in samples studied was not higher than 10^{-3} mass %. The YB_6 and LaB_6 samples have been obtained in an analogous way.

The ultrasound studies were performed on samples which were cut from the zone-melted single crystals. The single crystals were grown using correspondingly oriented seeds. According to the x-ray topography and Laue photograph analysis, their real structures are highly perfect. Electron diffraction and high-resolution transmission microscopy analysis allowed us to determine the characteristics of local structural details of the single crystals: according to the electron Kikuchi patterns and point electron diffraction patterns, which correspond only to the UB_{12} or CaB_6 type structures, defects were practically absent.

The sound velocity measurements in borides were performed at the liquid nitrogen temperature along the principal crystallographic axes by employing the phase-frequency method within the frequency range of 53–55 MHz. In this method the phase shift in a sample can be represented by

$$\Phi = 2\pi fL / s = 2\pi n + \delta\varphi , \qquad (1)$$

where f is frequency, s is velocity of the sound, L is thickness of a sample, $n \geq 0$ is integer number. For the studied samples $L \sim 3$–10 mm and $s \sim (6-10)\cdot 10^5$ cm/s, i.e., the value of n is estimated to be about 10–100. In the first stage, the sound velocity was estimated from a slope of the phase-frequency characteristic of a sample, $d\Phi / df = 2\pi L / s$, measured by the difference method. This procedure permitted to eliminate the phase shifts introduced by piezotransducers and feeders. For $n > 30$, corresponding to large L and small s, such measurements allowed to obtain immediately the sound velocity with acceptable accuracy. In the opposite case, this first stage provided the exact value of n, and thereafter s can be evaluated from $\delta\varphi$ value (see Ref. 29 for more details). By this means the accuracy of sound velocity measurements for the borides (Table 1) is estimated to be not worse than 0.5%.

In order to obtain all main elastic constants in a cubic crystal, one needs to measure the velocities of three eigen modes as sound propagates along C_2 axis [30]. These modes are

$$C_{44}\ (\mathbf{q} \,||\, [110], \mathbf{u} \,||\, [001]),$$
$$(C_{11} - C_{12})/2\ (\mathbf{q} \,||\, [110], \mathbf{u} \perp [001]),$$
$$C' = (C_{11} + C_{12})/2 + C_{44}\ (\mathbf{q} \,||\, [110], \mathbf{u} \,||\, [110]).$$

Here $\mathbf{q}$ is the wave vector, $\mathbf{u}$ is the polarization. Then the velocity s_4 of the C_{11} mode can be evaluated as $s_{4,\mathrm{calc}} = \sqrt{s_2^2 + s_3^2 - s_1^2}$. However, here we measured the velocity of the C_{11} mode directly ($\mathbf{q} \,||\, [100]$, $\mathbf{u} \,||\, [100]$). This allowed to obtain more accurately values of the C_{11} mode velocities and, in addition, to verify our measurements at $\mathbf{q} \,||\, [110]$ by comparing measured and calculated values of s_4 (the last two columns in Table 1). It is clearly seen, that the discrepancies between these values are well within the accepted accuracy of our measurements.

Table 1. Sound velocities in borides (in 10^5 cm/s) measured at $T = 78$ K.

Compound	Sound velosities				
	s_1 **q** ||[110], **u** ||[001]	s_2 **q** ||[110], **u** ⊥ [001]	s_3 **q** ||[110], **u** ⊥ [110]	s_4 **q** ||[100], **u** ||[100]	
				exp.	calc.
YB_6	3.11	7.47	—	10.77	—
LaB_6	4.35	6.6	—	9.9	—
ZrB_{12}	8.56	6.6	12.3	11.1	10.98
HoB_{12}	7.3	5.9	10.5	9.6	9.56
ErB_{12}	7.48	5.91	10.6	9.6	9.57
TmB_{12}	7.28	5.8	10.6	9.7	9.64
LuB_{12}	7.71	5.8	10.9	9.62	9.61

Table 2. Elastic constants of borides measured at $T = 78$ K.

Compound	Elastic constants							
	ρ, g / cm^3	C_{11}, GPa	C_{44}, GPa	C_{12}, GPa	B, GPa	ν	A_Z	Θ_D, K
YB_6	3.706	430	36	16	154	0.036	0.17	650, 706 [8]
LaB_6	4.710	463	89	45	184	0.089	0.43	770
ZrB_{12}	3.612	443	265	129	234	0.226	1.69	1260, 1000 [5]
HoB_{12}	4.655	429	248	105	213	0.197	1.53	1085
ErB_{12}	4.706	434	263	105	214	0.195	1.60	1100
TmB_{12}	4.756	448	252	128	233	0.222	1.58	1080
LuB_{12}	4.868	450	290	123	232	0.215	1.77	1110, 1190 [28]

$B = (C_{11} + 2C_{12})/3$ is the bulk modulus, $\nu = C_{12}/(C_{11} + C_{12})$ is the Poisson ratio, $A_Z = 2C_{44}/(C_{11} - C_{12})$ is Zener's elastic anisotropy parameter, Θ_D is the Debye temperature (present work and specific heat data of Refs. 5, 8, 28), ρ is the x-ray density.

The evaluated elastic constants, bulk moduli, and Debye temperatures of the borides are given in Table 2. The Debye temperatures were calculated according to the relationship (Ref. 30, in Gauss units):

$$\Theta_D = 0.0036265\left(\frac{\rho z}{AI}\right)^{1/3},$$

where ρ is the x-ray density, A is the molecular weight, z is the number of oscillators in the molecule (we assumed $z = 13$ and $z = 7$ for dodecaborides and hexaborides, respectively), I is the sum of inverse cubes of the elastic waves velocities, averaged over all directions of the wave normal [30]. The obtained by this way values of Θ_D are in agreement with the results of specific heat studies in ZrB_{12} [5], LuB_{12} [28], and YB_6 [6] (see Table 2). The measured lattice parameters are listed in Tables 3 and 4. These values appeared to be in accordance with the previously published data (see. Ref. 3 and references therein).

Table 3. Experimental and theoretical values of lattice constants and bulk moduli of MB_6 hexaborides.

Compound	a_{exp}, Å	a_{theor}, Å	B_{exp}, GPa	B_{theor}, GPa
CaB_6	4.152 [3]	4.131	—	159
SrB_6	4.197 [3]	4.166	—	160
BaB_6	4.269 [3]	4.230	—	162
EuB_6	4.1845	4.164	167 [13]	159
YbB_6	4.1468 [3]	4.079	166 [13]	159
YB_6	4.1002	4.080	154, 189 [44]	179
LaB_6	4.1565	4.130	184, 170 [13], 186 [43]	184
CdB_6	4.1066 [3]	4.112	170 [43]	175

Table 4. Experimental and theoretical values of lattice constants and bulk moduli of MB_{12} dodecaborides.

Compound	a_{exp}, Å	a_{theor}, Å	B_{exp}, GPa	B_{theor}, GPa
YB_{12}	7.500	7.45	—	224
ZrB_{12}	7.4077	7.331	234	249
HoB_{12}	7.4923	7.45	213	215
ErB_{12}	7.4841	7.443	214	217
TmB_{12}	7.4752	7.424	233	220
LuB_{12}	7.4644	7.413	232	223
HfB_{12}	7.377 [3]	7.349	—	243
ThB_{12}	7.612 [3]	7.543	—	239
UB_{12}	7.470 [3]	7.399	249 [45]	250

Details of calculations

The hexaborides crystallize in the CaB_6-type cubic crystal structure which can be described in terms of the CsCl lattice, where M atoms occupy Cs sites, and the B_6 octahedra are situated in the Cl sites. The basic structural elements of the cubic dodecaborides are stable cuboctahedral B_{12} clusters. The corresponding UB_{12}-type structure is similar to the simple rock-salt lattice, where M atoms and B_{12} cuboctahedrons occupy the Na- and Cl-sites, respectively.

The *ab initio* electronic structure calculations were carried out for the paramagnetic (PM), ferromagnetic (FM), and antiferromagnetic (AFM) phases of MB_6 and MB_{12} by using the density functional theory in the local spin density approximation (LSDA) and the generalized gradient approximation (GGA) in the framework of the relativistic full potential linear muffin-tin orbital (FP-LMTO) method [31–33]. In contrast to previous band-structure calculations for borides (see, e.g., Refs. 20, 25), which were mainly based upon atomic sphere approximation (ASA) techniques, in the present FP-LMTO method one can avoid extra shape approximations imposed on the charge density or potential. The main details of the FP-LMTO method employed in the present work are given in Refs. 31–33.

In RE compounds the localized strongly correlated $4f$ electrons still present a challenge to the band theory [34,35]. The results of first-principles calculations together with a wealth of experimental data (including bulk and Fermi surface properties) indicate, that in order to describe the ground state of RE compounds, it is feasible to consider the $4f$ states as semi-localized core states, in line with Refs. 34, 35. Actually, the standard RE model [34] is employed in this work in the limit of the large Hubbard repulsion U within the *ab initio* LSDA and GGA schemes for the exchange-correlation effects. In other words, the localized $4f$ states of RE are treated as spin-polarized outer-core wave functions, contributing to the total spin density, and the spin occupation numbers were fixed by applying the Russel–Saunders coupling scheme to the $4f$ shell, which was not allowed to hybridize with conduction electrons.

The band structures of MB_6 and MB_{12} were calculated self-consistently for a number of lattice parameters close to experimental ones. The bulk moduli B and the theoretical lattice parameters a are evaluated according to Ref. 31 from the calculated total energies as functions of volume, i.e. from the corresponding equations of states (EOS) $E(V)$, and listed in Tables 3 and 4. For metallic MB_6 and MB_{12} compounds the calculated total and partial densities of electronic states (DOS) at the Fermi level, $N(E_F)$, are given in Table 5.

In addition, to investigate the chemical bonding in hexa- and dodecaborides, the balanced crystal orbital overlap populations (BCOOP) [33] have been calculated for a number of the borides within the FP-LMTO technique. The BCOOP is defined as the orbital population weighted density of states with a «balancing» denominator [33], and this method is similar to the well known COOP, which is the solid-state generalization of the quantum chemical quantity called overlap population. The original COOP appeared to be a basis set dependent quantity, and in the limit of nearly linear dependent basis set the COOP overestimates the antibonding character of electronic states (see Refs. 33 and references therein). However, the BCOOP method greatly suppresses the basis set dependence and treats the bonding and antibonding states on more or less equal footing, in a *balanced* way. The BCOOP is an energy resolved quantity which is positive for bonding states and negative for antibonding states. Therefore it allows to discriminate between bonding and antibonding contributions to the chemical bond.

Also, in order to shed light on the electronic structure of the mixed-valent SmB_6 and YbB_{12} compounds within the LSDA + U approach [36], the *ab initio* pseudo-potential VASP-PAW method has been employed in the present work (see Ref. 37 for details).

Table 5. Total and partial densities of electronic states at E_F for MB_6 and MB_{12} compounds.

DOS states/Ry·f.u.	Compound								
	MB_6					MB_{12}			
	Y	La	Gd	Eu (PM)	Eu (FM)	Y	Zr	Lu	U
M_s	0.23	0.10	0.14	0.00	0.00	0.04	0.07	0.05	0.02
M_p	0.13	0.13	0.04	0.00	0.00	0.02	0.07	0.02	0.68
M_d	6.81	4.90	5.93	0.27	0.35	4.41	6.60	4.21	2.09
M_f	1.19	3.72	0.19	0.01	0.06	1.24	1.79	1.15	65.63
B_s	0.25	0.14	0.29	0.02	0.02	0.37	0.57	0.40	0.43
B_p	2.88	3.07	3.29	0.52	1.87	7.65	8.87	7.49	14.52
Total	11.49	12.06	9.88	0.82	2.30	13.73	17.97	13.32	83.37
$N^{\gamma}_{\rm exp}(E_F)$	23.4 [8]	14.2 [40]	—	—	—	18.0 [28]	25.5 [5]	23.8 [28]	116 [41]

Results and discussion

MB_6

There is no agreement on the nature of FM in the La-doped CaB_6 and SrB_6: either it is the FM phase of a dilute electron gas (see, e.g., Ref. 19), or it is related to the presumed excitonic state [38], or be caused by distortions and vacancies of whole B_6 clusters [23]. At the same time, the features of band overlap, or the presence of a small energy gap, have important implications for the models proposed to explain the magnetic properties of these borides [20,22,38].

The total and partial densities of electronic states $N(E)$ for CaB_6, calculated for experimental values of lattice constants and atomic positions, as well as the corresponding principal BCOOPs, are shown in Fig. 1. It should be pointed out, that we also obtained very similar DOS and BCOOP for the isovalent alkaline-earth hexaborides, SrB_6 and BaB_6. In Fig. 1 one can clearly see bonding valence states, which are separated from the antibonding states of the conduction band by a small energy gap. However, the calculated BCOOP and the valence charge density indicate, that the chemical bonding in CaB_6 is more complex. Whereas the B–B bonds are predominantly covalent, the Ca–B bonds demonstrate a substantial ionic character.

Our calculations have also revealed, that for experimental values of lattice constants and atomic positions

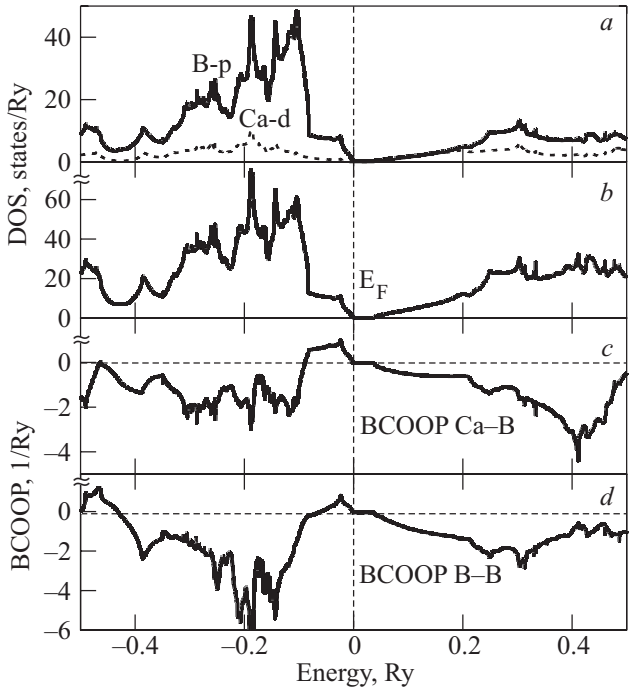

Fig. 1. Calculated densities of states and balanced crystal orbital overlap populations for CaB_6: (*a*) partial boron *p* (solid line) and calcium *d* (dashed line) DOS; (*b*) total DOS; (*c*) Ca–B BCOOP; (*d*) B–B BCOOP.

the stoichiometric CaB_6, SrB_6, and BaB_6 are semiconductors with small energy gaps: 0.48, 0.16, and 0.02 eV, correspondingly. These results are in a qualitative agreement with the recently obtained angle-resolved photoemission spectroscopy (ARPES) data [22], indicating that CaB_6 is a semiconductor with the energy gap of about 1 eV. The difference between experiment and calculations would be expected, since the LDA calculations usually yield underestimated energy gaps. Previous band structure calculations, based on the LDA and ASA, provided semimetallic spectra for CaB_6, SrB_6, and BaB_6 [20,25], whereas employment of the quasiparticle *GW* approximation has given both semiconducting [20] and semimetallic [21] ground states for the divalent hexaborides. These contradictory results show that fine details of the band structure of hexaborides are very sensitive to specific implementations of *ab initio* techniques.

Also, a value of the energy gap in alkaline-earth hexaborides is found to be related to the positional parameter X, which governs the difference between intra- and inter-octahedral B–B distances. These different B–B bond lengths become equal at $X = 0.207$, and for this case the calculations provide the largest values of the energy gaps. Note, that experimental studies usually yield $X < 0.207$, and the difference between calculated values of the energy gap, or even its absence, can be related to a chosen value of parameter X.

Though the EuB_6 compound is also a divalent hexaboride, its transport and magnetic properties are complex and different from those of alkaline-earth hexaborides. The EuB_6 orders partially ferromagnetically at 15 K, then the resistivity and specific heat show another phase transition at 12.5 K, with the majority of Eu spins become ferromagnetically aligned [14]. Here we did not address the origin of these phase transitions, as it lies beyond the aim of the present paper and capabilities of the methods employed. Instead, the detailed electronic structure calculations were carried out to shed light on the ground state of EuB_6, and to provide a reliable basis for further analysis of its peculiar properties.

According to our calculations, EuB_6 is found to be semimetallic in both paramagnetic and FM phases (see the corresponding $N(E_F)$ in Table 5), and the higher value of $N(E_F)$ for the FM phase appeared to be in conformity with the observed temperature behavior of resistivity [13,14]. Also, the total energy appeared to be minimal precisely for the FM phase. It should be noted, however, that the spin polarization of the $4f$ states of Eu does not influence substantially the electronic structure of EuB_6, and the energy splitting between minority and majority bands is very small in the vicinity of E_F. As a result, the calculated magnetic moment of EuB_6, $7.03\mu_B$, is completly due to the half-filled $4f$ shell, and the contribution of conduction electrons to the moment is very small.

For YbB_6 hexaboride we have obtained the semiconducting ground state with a tiny energy gap of about 0.05 eV. The assumed Yb^{2+} state is in agreement with the estimations of Ref. 16, which indicate that 2% of the Yb ions presumably adopt Yb^{3+} configuration, and the rest of Yb ions are divalent. According to our calculations, the trivalent Yb^{3+} state would correspond to substantially higher total energy for YbB_6, and the origin of the recently reported weak FM in YbB_6 [16] is not clear.

Among trivalent metallic hexaborides the nonmagnetic YB_6 and LaB_6 compounds are superconductors with transition temperatures of about 7 and 0.1 K, respectively [1]. The calculated DOS (total and partial) and BCOOP for YB_6 and LaB_6 are shown in Figs. 2 and 3, respectively. One can see that main features of the $N(E)$ curves are similar to those calculated for the divalent CaB_6 (Fig. 1). The occupied energy bands are formed by hybrid boron 2*s*–2*p* states, related to the inter- and intra-octahedral B–B bonds. The highest fully occupied bands are formed by *p* states responsible for the inter-octahedral interactions. The partially occupied band contains a substantial contribution from cation states and has also a large dispersion, which reflects the delocalized character of *p* and *d* states at the bottom of the conduction band. As a result, there are two fairly broad peaks in $N(E)$ of hexaborides, corresponding to bonding and antibonding states and arising due to hybridization of *d* states of metal and *p* states of boron in predominantly covalent B–B bonds inside and between B_6 clusters. In general, the calculated band structure of YB_6 is in agreement with the results of Ref. 39.

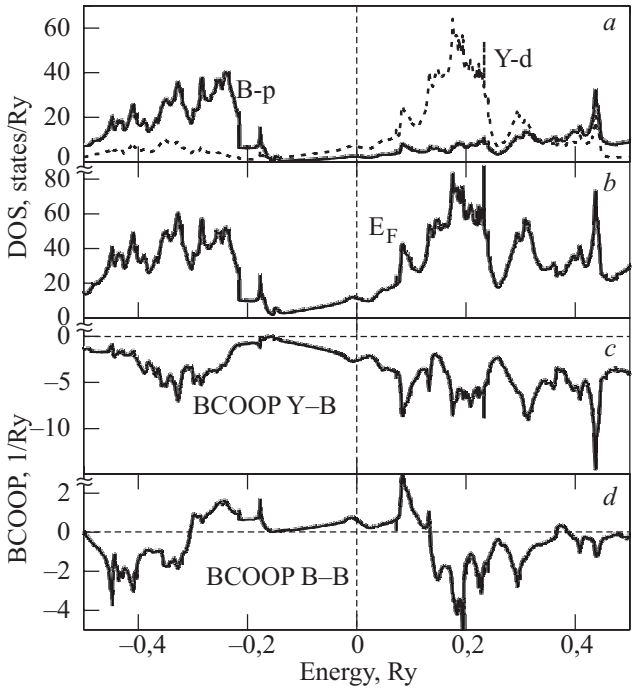

Fig. 2. Calculated densities of states and balanced crystal orbital overlap populations for YB_6: (*a*) partial boron *p* (solid line) and yttrium *d* (dashed line) DOS; (*b*) total DOS; (*c*) Y–B BCOOP; (*d*) B–B BCOOP.

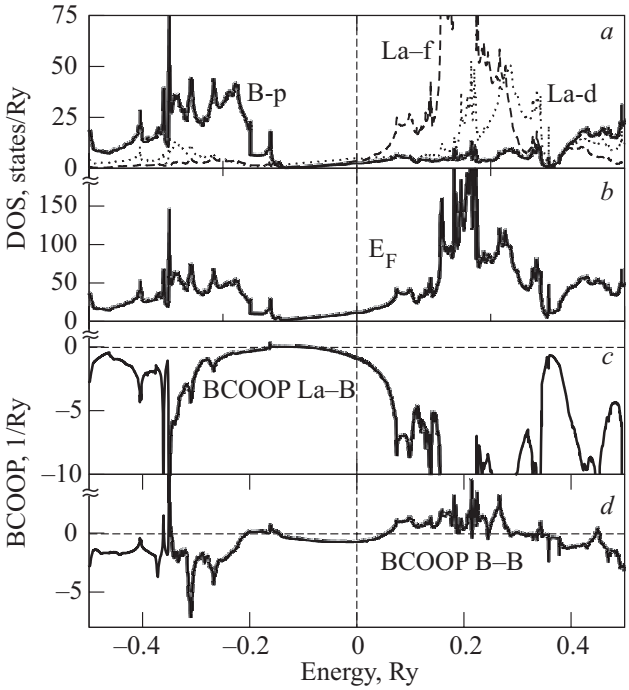

Fig. 3. Calculated densities of states and balanced crystal orbital overlap populations for LaB_6: (*a*) partial boron *p* (solid line), lanthanum *d* (dotted line) and *f* (dashed line) DOS; (*b*) total DOS; (*c*) La–B BCOOP; (*d*) B–B BCOOP.

However, there are also notable distinctions between electronic structures of YB_6 and LaB_6. As can be seen in Fig. 3 and Table 5, the 4*f* states of La give a substantial contribution to DOS in LaB_6 at the Fermi level, $N(E_F)$, and this provides the highest value of $N(E_F)$ among trivalent hexaborides. On the other hand, the aggregate of non-*f*-partial contributions to $N(E_F)$ is found to be higher in case of YB_6 (see Table 5). Presumably, the sharp dissimilarity between SC transition temperatures of YB_6 and LaB_6 (7 K against 0.1 K, respectively) can be related to a difference in symmetry of electronic states at E_F, and in the corresponding composition of partial contributions to $N(E_F)$. There is also a clearly seen «bump» in the $N(E)$ curve at E_F for YB_6 (see Fig. 2), whereas analogous feature is barely noticed in $N(E)$ for LaB_6 in Fig. 3.

The calculated $N(E_F)$ can be compared with the corresponding «experimental» values taken from the measured electronic specific heat coefficients, $\gamma = 2\pi^2 k_B^2 N^{\gamma}_{\rm exp}(E_F)/3$ (see Table 5). For this comparison, the calculated «bare» $N(E_F)$ have to be enhanced, presumably due to the electron–phonon interaction: $N^{\gamma}_{\rm exp}(E_F) = (1+\lambda)N(E_F)$. This provides the estimations of many-body enhancement factors, $\lambda = 1.0$ and $\lambda = 0.2$

for YB_6 and LaB_6, respectively, which can contribute to the observed sharp difference in SC properties of these compounds. On the other hand, it was recently reported [42] that YB_6 can not be definitively classified as either «exotic» or «conventional» superconductor, but instead this compound displays behavior which interpolates between the two regimes.

Another distinction between yttrium and lanthanum hexaborides resides in the chemical bonding. As one can see from the BCOOP plots in Fig. 2, the yttrium–boron bonding in YB_6 is of an ionic character, whereas the B–B bonding, as in the case of CaB_6, has covalent features. This is also in agreement with the calculated charge density distribution for YB_6, given in Fig. 4, where one can see no covalent bonds involving Y atoms. For the isoelectronic LaB_6 the calculated BCOOP in Fig. 3 also demonstrates a clear picture of ionic bonding between La and B atoms, whereas there are no conspicuous covalent bonds between boron atoms. This suggests that the B–B bonding has some traits of metallic character, as well as weak La–La bonds, and therefore such bonding can be related to the high electron emissivity and low work function of LaB_6.

As can be seen in Table 3, the calculated bulk moduli of MB_6 are in a fair agreement with the available experimental data. It should be noted, however, that the listed in Table 3 bulk moduli of EuB_6 (167 GPa) and YB_6 (189 GPa) were estimated in Refs. 13 and 14 by interpolation, and these values should be used with great caution. Also, one can see in Table 3, that calculated values of bulk moduli for the trivalent hexaborides appeared to be about 10% larger than the theoretical B of the divalent hexaborides. The Poisson ratio, $\nu = C_{12}/(C_{11}+C_{12})$, is found to be very small for LaB_6 and, especially, for YB_6 (see Table 2) because of the large C_{11} and the small C_{12} values.

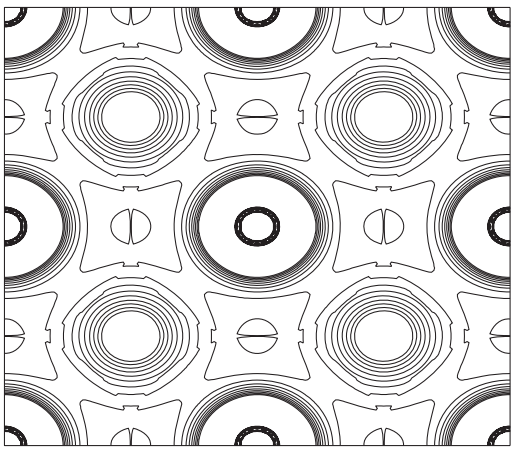

Fig. 4. Charge density for YB_6 hexaboride in the plane crossing through the Y atoms. Sections through the boron bonds are also seen.

On the other hand, for the divalent hexaborides EuB_6 and YbB_6 ν are expected to be higher, about 0.1 and 0.2, respectively, due to larger values of C_{12} (see Ref. 13). For all MB_6 compounds the Cauchy relation, $C_{12} = C_{44}$, is not fulfilled, and this indicates noncentral force bonding, in accordance with the calculated BCOOPs. To characterize elastic anisotropy of a crystal, one usually employs Zener's anisotropy parameter, $A_Z = 2C_{44}/(C_{11}-C_{12})$, which is close to 1 for an isotropic solid. As can be seen in Table 2, A_Z is substantially smaller than 1 in YB_6 and LaB_6, and this trend is expected to hold true for the whole MB_6 series.

MB_{12}

For the reference dodecaboride YB_{12} the calculated DOS and BCOOP are presented in Fig. 5. Very similar plots were obtained for the isovalent LuB_{12} compound. In general, the band structure of trivalent dodecaborides is determined by hybridization of the valence s, p, d states of the metallic element with the $2p$ states of boron. There are two groups of hybrid bands, separated by a «pseudogap» with substantial dispersion in the electronic spectrum at E_F. As is seen from the BCOOP plots in Fig. 5, the yttrium–boron bonding is of an ionic character, whereas the B–B bonding does not reveal a distinct picture of strong covalent bonds. Instead the B–B BCOOP is negative at low energies, then becomes positive, and at high energies it is negative again.

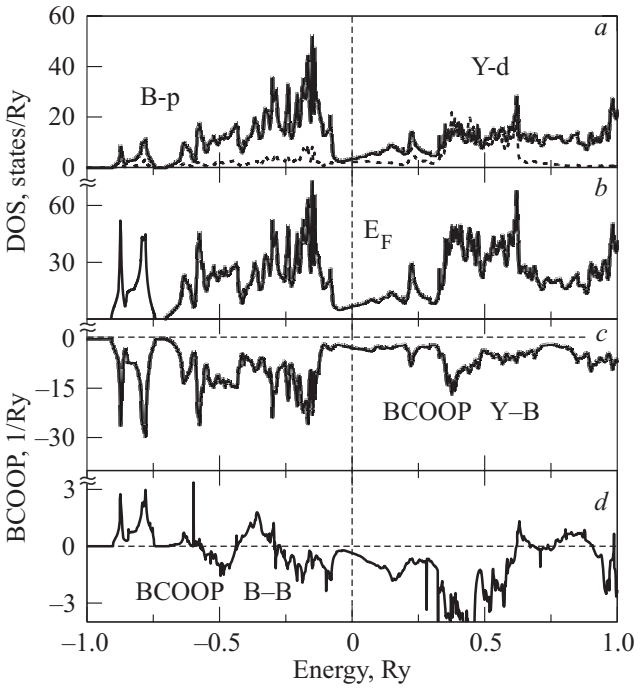

Fig. 5. Calculated densities of states and balanced crystal orbital overlap populations for YB_{12}: (*a*) partial boron p (solid line) and yttrium d (dashed line) DOS; (*b*) total DOS; (*c*) Y–B BCOOP; (*d*) B–B BCOOP.

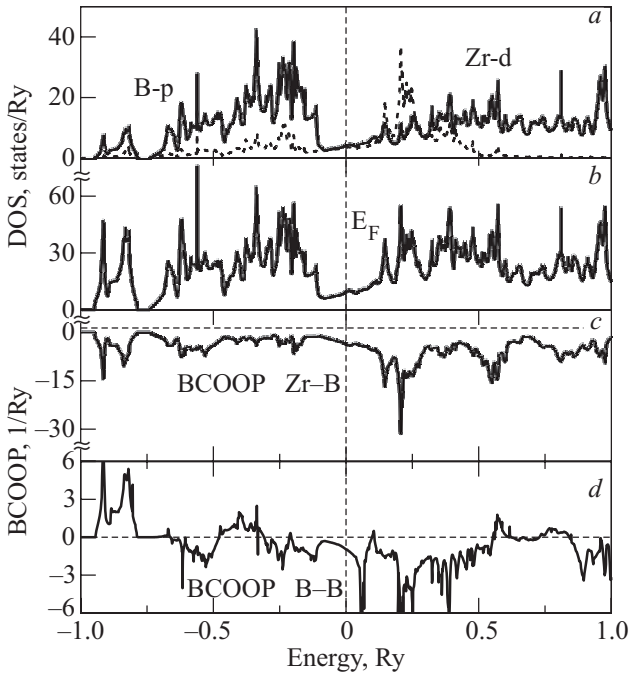

Fig. 6. Calculated densities of states and balanced crystal orbital overlap populations for ZrB_{12}: (*a*) partial boron *p* (solid line) and zirconium *d* (dashed line) DOS; (*b*) total DOS; (*c*) Zr–B BCOOP; (*d*) B–B BCOOP.

For the ZrB_{12} compound the calculated DOS and BCOOP in Fig. 6 are similar to the corresponding ones in YB_{12}, and slight distinctions in their spectra are related to the larger band filling in ZrB_{12}. The BCOOP in Fig. 6 also demonstrates the clear picture of ionic bonding between Zr and B atoms, whereas the bonds between boron atoms are complicated, covalent with, perhaps, small mixture of metallic character. This model of the bonding is consistent with the calculated charge density distribution for ZrB_{12} in Fig. 7.

In contrast to YB_6, the *p* electrons of boron provide the main contribution to the DOS of YB_{12} at E_F, whereas the contribution from *d* electrons of yttrium appears to be comparatively small (see Fig. 5 and Table 5). On the other hand, in superconducting ZrB_{12} the partial contribution of *d* electrons to $N(E_F)$ is found to be larger than the corresponding contributions in YB_{12} and LuB_{12}. In Fig. 6 one can see a clear «bump» in $N(E)$ of ZrB_{12} at E_F, similar to the peak revealed in the DOS of superconducting YB_6 (see Fig. 2).

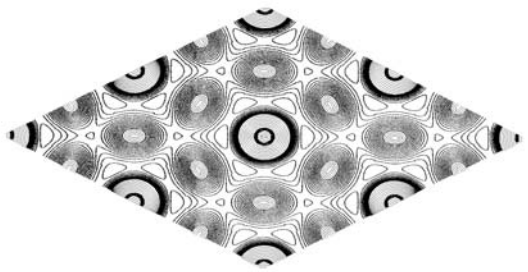

Fig. 7. Charge density for ZrB_{12} in the plane crossing through Zr atoms. Sections through the boron bonds are also seen.

The detailed analysis of SC in borides apparently goes beyond the aim of the present work, but it seems likely that substantial presence of *d* electrons at E_F is favorable for SC of YB_6 and ZrB_{12}. Also, estimated from the calculated $N(E_F)$ and experimental electronic specific heat data in Table 5, the electron–phonon coupling constants are found to be $\lambda = 1.0$ and $\lambda = 0.42$ in YB_6 and ZrB_{12}, respectively. This attracts attention to the origin of SC in ZrB_{12}, which is a widely debated topic [4–7].

As can be seen in Table 5, in UB_{12} the 5*f* states of uranium yield a dominant contribution to DOS at E_F, providing the highest value of total $N(E_F)$ among dodecaborides. This value is in agreement with the experimental electronic specific heat data of Ref. 41, provided the electron–phonon coupling constant $\lambda = 0.4$ is accepted. This confirms the itinerant *f*-electron picture for UB_{12}, in which neither SC nor magnetic ordering was detected [41].

The theoretical and experimental values of the bulk moduli and the lattice parameters of MB_{12} are listed in Table 4. Taking into account the over-binding tendency of the LDA [31], which generally provides smaller lattice parameters and higher bulk moduli, one can see that the calculated *B* and *a* are in good agreement with the experimentally observed trends in the MB_{12} series. In particular, the lattice parameters decrease slightly in a linear fashion in the series of HoB_{12}, ErB_{12}, TmB_{12}, and LuB_{12} due to the lanthanide contraction. It is also seen in Table 4, that the bulk moduli are expected to be higher for compounds which have more electrons in the conduction band, i.e. for ZrB_{12}, HfB_{12}, and UB_{12}, as compared to MB_{12} with the trivalent (specifically RE) metals. For the dodecaborides the Poisson ratio ν appeared to be close to 0.2 (see Table 2), whereas $\nu \le 0.1$ for the trivalent hexaborides. As to the elastic anisotropy parameter A_Z, it lies between 1.5 and 1.8 for the MB_{12} series as opposed to $A_Z \le 0.5$ in MB_6, though the deviations from the isotropic value $A_Z \simeq 1$ hold true in both series. As in the case of hexaborides, we note a departure from the Cauchy relation, $C_{12} = C_{44}$, which is attributed to the noncentral force bonding. This is in accordance with the calculated BCOOPs for MB_{12}.

In the present study a particular attention has been given to the famous Kondo insulator YbB_{12}, where the origin of the observed tiny energy gap (about 30 meV) remains controversial, both experimentally and theoretically [9–11,38]. In Ref. 9 a small hybridization gap was obtained for YbB_{12} within the LDA + *U* approach assum-

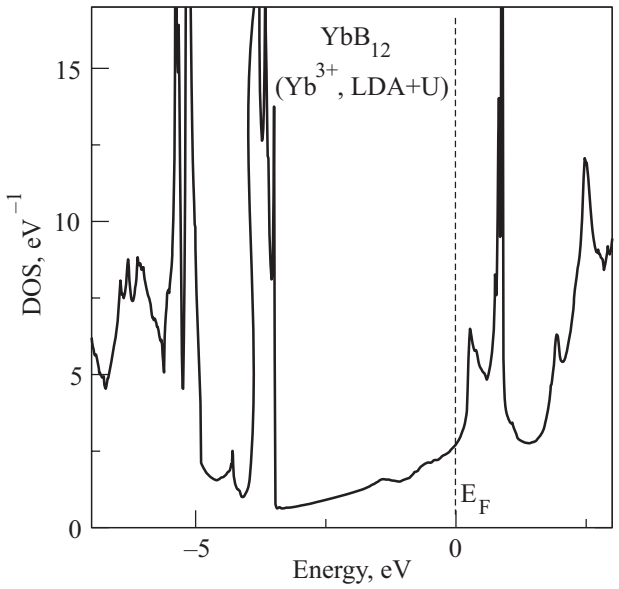

Fig. 8. Total density of states for YbB_{12} calculated within the LSDA + U approach.

ing the *divalent* state of Yb ion. On the other hand, a wealth of experimental data indicate the valence state close to Yb^{3+} in YbB_{12} (see, e.g., Ref. 10 and references therein).

Here we tried to reach a true band theory limit in order to explain the experimental data and to explore a possibility of the hybridization gap in YbB_{12}. For the Yb^{3+} state of ytterbium, we have employed the LSDA + U approach in the framework of the VASP-PAW method [37]. The resulting DOS in Fig. 8 represents 13 hybridized 4f energy bands below the Fermi energy (E_F), and the 14th empty state just above E_F with no hybridization gap. Even taking into consideration some uncertainty in deciding on a particular value of parameter U (6 and 7 eV were actually tried here), one can consider the obtained configuration in Fig. 8 as relevant to the formation of a Kondo singlet and compatible with an excitonic instability scenario of Ref. 38.

Obviously, our FP-LMTO LSDA and GGA calculations have not provided the energy gap for PM, FM, and AFM phases of $Yb^{3+}B_{12}$. However, for YbB_{12} the detailed calculations of the equation of state, $E(V)$, for different spin configurations point to a predominantly AFM coupling between Yb^{3+} ions. Specifically, the calculated ground state total energy for AFM configurations appeared to be about 20 meV lower than the energy of the paramagnetic state. This is consistent with the recent neutron scattering spectrum studies for YbB_{12} [10,11], where the sharp 15 meV peak in the low-energy peak structure has been attributed to Yb–Yb AFM correlations in the PM state.

Summary

As a whole, the results of present electronic structure calculations for MB_6 and MB_{12} are in agreement with the available experimental data on low temperature and bulk properties of higher borides. Our calculations confirm a semiconducting ground state of CaB_6, SrB_6, and YbB_6 with the lower estimations for the energy gaps of 0.5, 0.2, and 0.05 eV, correspondingly, whereas a small overlap between conduction and valence bands is found in EuB_6.

For metallic $R^{3+}B_x$ borides the calculated DOS(E_F) are in agreement with the electronic specific heat and T_{SC} trends. In YB_6 the electron–phonon interaction is estimated to be strong enough to provide the observed superconducting transition temperature of 7 K. The itinerant f-electron picture is confirmed for UB_{12}.

For the first time the elastic constants of a series of dodecaborides (ZrB_{12}, HoB_{12}, ErB_{12}, TmB_{12}, and LuB_{12}) and hexaborides (YB_6 and LaB_6) were evaluated with one single experimental technique, and compared with the results of *ab initio* calculations. The calculated bulk moduli are in agreement with the experimentally observed trends in the MB_6 and MB_{12} series. In particular, the bulk moduli are expected to be higher for borides which possess more electrons in the conduction band.

Our calculations have shown that the bonding picture in the majority of MB_6 and MB_{12} compounds can be considered as a mixture between covalent, metallic and ionic bonding. In particular, the BCOOP has been evaluated as a measure of the bonding character and a complementary quantity to the charge density analysis. Eventhough the BCOOP in the B–B case displays mostly covalent features, both for MB_6 and MB_{12}, it does not justify the consideration of these bonds as being purely covalent.

The calculated total energy for the AFM configuration of YbB_{12} is about 20 meV lower than for the paramagnetic state. This is consistent with the neutron scattering spectrum studies for YbB_{12} by Alekseev et al. [10,11], where a sharp 15 meV peak has been attributed to Yb–Yb AFM correlations.

We are grateful to P.A. Alekseev, K. Flachbart, A.G. Grechnev, K. Siemensmeyer, N.E. Sluchanko, I.V. Svechkarev, and O.J. Żogal for fruitful scientific discussions.

This work has been supported by the Swedish Research Council (VR) and the Foundation for Strategic Research (SSF), by INTAS project 03-51-3036, and by the Russian–Ukrainian RFBR-NASU project 8-2008.

1. B.T. Matthias, T.H. Geballe, K. Andres, E. Corenzwit, G.W. Hull, and J.P. Maita, *Science* **159**, 538 (1968).
2. J. Etourneau and P. Hagenmuller, *Philos. Mag.* **B52**, 589 (1985).
3. *Handbook of High Temperature Compounds: Properties, Production, Applications*, T.Ya. Kosolapova (ed.), Hemisphere Pub. Corp., New York (1990).

4. M.I. Tsindlekht, G.I. Leviev, I. Asulin, A. Sharoni, O. Millo, I. Felner, Yu.B. Paderno, V.B. Filippov, and M.A. Belogolovskii, *Phys. Rev*. **B69**, 212508 (2004).
5. R. Lortz, Y. Wang, S. Abe, C. Meingast, Yu.B. Paderno, V. Filippov, and A. Junod, *Phys. Rev.* **B72**, 024547 (2005).
6. R. Khasanov, D. Di Castro, M. Belogolovskii, Yu. Paderno, V. Filippov, R. Brütsch, and H. Keller, *Phys. Rev*. **B72**, 224509 (2005).
7. V.A. Gasparov, N.S. Sidorov, and I.I. Zver'kova, *Cond-mat/0508151* (2005).
8. R. Lortz, Y. Wang, U. Tutsch, S. Abe, C. Meingast, P. Popovich, W. Knafo, N. Shitsevalova, Yu.B. Paderno, and A. Junod, *Phys. Rev*. **B73**, 024512 (2006).
9. V.N. Antonov, B.N. Harmon, and A.N. Yaresko, *Phys. Rev.* **B66**, 165209 (2002).
10. P.A. Alekseev, J.-M. Mignot, K.S. Nemkovski, E.V. Nefeodova, N.Yu. Shitsevalova, Yu.B. Paderno, and R.I. Bewley, *J. Phys.: Condens. Matter* **16**, 2631 (2004).
11. J.M. Mignot, P.A. Alekseev, K.S. Nemkovskii, L.P. Regnault, F. Iga, and T. Takabatake, *Phys. Rev. Lett*. **94**, 247204 (2005).
12. J.L. Gavilano, B. Ambrosini, P. Vonlanthen, H.R. Ott, D.P. Young, and Z. Fisk, *Phys. Rev. Lett*. **81**, 25 (1998).
13. S. Zherlitsyn, B. Wolf, B. Luthi, M. Lang, P. Hinze, E. Uhrig, W. Assmus, H.R. Ott, D.P. Young, and Z. Fisk, *Eur. Phys. J.* **B22**, 327 (2001).
14. J. Kunes and W.E. Pickett, *Phys. Rev*. **B69**, 165111 (2004).
15. J.M. Tarascon, J. Etourneau, P. Dordor, P. Hagenmuller, M. Kasaya, and J.M.D. Coey, *J. Appl. Phys*. **51**, 574 (1980).
16. J.L. Gavilano, S. Mushkolaj, D. Rau, H.R. Ott, A. Bianchi, and Z. Fisk, *Physica* **B329–333**, 570 (2003).
17. M. Takeda, T. Fukuda, F. Domingo, and T. Miura, *J. Solid State Chem.* **177**, 471 (2004).
18. D.P. Young, D. Hall, M.E. Torelli, Z. Fisk, J.L. Sarrao, J.D. Thompson, H.-R. Ott, S.B. Oseroff, R.G. Goodrich, and R. Zylser, *Nature* **397**, 412 (1999).
19. J. Akimitsu, K. Takenawa, K. Suzuki, H. Harima, and Y. Kuramoto, *Science* **293**, 1125 (2001).
20. H.J. Tromp, P. van Gelderen, P.J. Kelly, G. Brocks, and P.A. Bobbert, *Phys. Rev. Lett*. **87**, 016401 (2001).
21. H. Kino, F. Aryasetiawan, K. Terakura, and T. Miyake, *Phys. Rev*. **B66**, 121103 (2002).
22. S. Souma, H. Komatsu, T. Takahashi, R. Kaji, T. Sasaki, Y. Yokoo, and J. Akimitsu, *Phys. Rev. Lett.* **90**, 027202 (2003).
23. T. Jarlborg, *J. Phys.: Condens. Matter* **15**, L249 (2003).
24. Z. Wu, D.J. Singh, and R.E.Cohen, *Phys. Rev.* **B69**, 193105 (2004).
25. S.-P. Gao, J. Jiang, M. Cao, J. Zhu, and J. Yuan, *Phys. Rev.* **B69**, 214419 (2004).
26. A. Kohout, I. Batko, A. Czopnik, K. Flachbart, S. Matas, M. Meissner, Y. Paderno, N. Shitsevalova, and K. Siemensmeyer, *Phys. Rev.* **B70**, 224416 (2004).
27. A. Czopnik, N. Shitsevalova, A. Krivchikov, V. Pluzhnikov, Yu. Paderno, and Y. Onuki, *J. Solid State Chem*. **177**, 507 (2004).
28. A. Czopnik, N. Shitsevalova, V. Pluzhnikov, A. Krivchikov, Yu. B. Paderno, and Y. Onuki, *J. Phys.: Condens. Matter* **17**, 5971 (2005).
29. E.A. Masalitin, V.D. Fil, K.R. Zhekov, A.N. Zholobenko, and T.V. Ignatova, *Fiz. Nizk. Temp.* **29**, 93 (2003) [*Low Temp. Phys*. **29**, 72 (2003)]; see also *Cond-mat/0301183* (2003).
30. F.I. Fedorov, *Theory of Elastic Waves in Crystal*, Plenum Press, New York (1968).
31. O. Eriksson and J.M. Wills, in: *Electronic Structure and Physical Properties of Solids*, Hugues Dreysse (ed.), Springer, Berlin (2000).
32. G.E. Grechnev, R. Ahuja, and O. Eriksson, *Phys. Rev*. **B68**, 064414 (2003).
33. A. Grechnev, R. Ahuja, and O. Eriksson, *J. Phys.: Condens. Matter* **15**, 7751 (2003); A. Grechnev, S. Li, R. Ahuja, O. Eriksson, U. Jansson, and O. Wilhelmsson, *Appl. Phys. Lett.* **85**, 3071 (2004); P. Souvatzis, J.M. Osorio-Guillen, R. Ahuja, A. Grechnev, and O. Eriksson, *J. Phys.: Condens. Matter* **16**, 5241 (2004).
34. M.S.S. Brooks and B. Johansson, in: *Ferromagnetic Materials*, vol. 7, K.H.J. Buschow (ed.), North-Holland, Amsterdam (1993).
35. V.B. Pluzhnikov, A. Czopnik, G.E. Grechnev, N.V. Savchenko, and W. Suski, *Phys. Rev.* B**59**, 7893 (1999).
36. A.I. Liechtenstein, V.I. Anisimov, and J. Zaane, *Phys. Rev.* **B52**, R5467 (1995).
37. G. Kresse and D. Joubert, *Phys. Rev.* **B59**, 1758 (1999).
38. S. Curnoe and K.A. Kikoin, *Phys. Rev*. **B61**, 15714 (2000).
39. B. Jäger, S. Paluch, W. Wolf, P. Herzig, O.J. Żogal, N. Shitsevalova, and Y. Paderno, *J. Alloys Compd.* **383**, 232 (2004).
40. E.F. Westrum, Jr., J.T.S. Andrews, B.H. Justice, and D.A. Johnson, *J. Chem. Thermodynamics* **34**, 239 (2002).
41. M. Kasaya, F. Iga, K. Katoh, and T. Kasuya, *J. Magn. Magn. Mater.* **90**–**91**, 521 (1990).
42. A.D. Hillier and R. Cywinski, *Appl. Magn. Res.* **13**, 12 (1997).
43. S. Nakamura, T. Goto, S. Kunii, K. Iwashita, and A. Tamaki, *J. Phys. Soc. Jpn*. **63**, 623 (1994).
44. H.E. King, S.J. La Placa, T. Penny, and Z. Fisk, in: *Valence Fluctuations in Solids*, L.M. Falikov, M.B. Maple, and W. Hanke (eds.), North-Holland, Amsterdam (1981).
45. J.-P. Dancausse, E. Gering, S. Heathman, and U. Benedict, *J. Alloys Compd*. **189**, 205 (1992).
46. J. He, E. Wu, H. Wang, R. Liu, and Y. Tian, *Phys. Rev. Lett.* **94**, 015504 (2005).